Power Electronic Systems Laboratory

Loss Modelling of Inductive Components Employed in Power Electronic Systems

J. Mühlethaler
J.W. Kolar
A. Ecklebe

ETH

Eidgenössische Technische Hochschule Zürich
Swiss Federal Institute of Technology Zurich

Loss Modeling of Inductive Components Employed in Power Electronic Systems

J. Mühlethaler*, J. W. Kolar*, and A. Ecklebe†

*Power Electronic Systems Laboratory, ETH Zurich, Email: muehlethaler@lem.ee.ethz.ch
†ABB Switzerland Ltd., Corporate Research, CH-5405 Baden-Dättwil

Abstract—Loss models of inductive components are thoroughly investigated, thereby all different aspects of loss modeling are considered. The impact of peak-to-peak flux density ΔB, frequency f, DC premagnetization H_{DC}, temperature T, core shape, minor and major loops, flux waveform, and material on core loss calculation are considered. In order to calculate winding losses, formulas for round conductors and litz wires, each including skin- and proximity effects (including the influence of an air-gap fringing field) are included. A high level of accuracy is achieved by combining the best state-of-the-art approaches and by embedding newly-developed approaches into a novel loss calculation framework. The loss models are verified by FEM simulations and experimental measurements.

I. INTRODUCTION

The future trends in power electronic research are towards higher efficiency and higher power density. The reduction of size and weight of power electronic systems is driven by cost considerations, e.g. material economies, space availability, e.g. in the automotive environment, and increasing efficiency requirements, e.g. aircraft weight reductions. Furthermore, due to increasing energy costs and increased ecological awareness, a high power electronic system efficiency is also desirable. The increase of the power density often affects the efficiency: a trade-off between these two quality indexes exists.

Inductive components occupy a significant amount of space in today's power electronic systems, and furthermore, considerable losses occur in these components. In order to increase the power density and/or efficiency of power electronic systems, losses in inductive components must be reduced, and/or new cooling concepts need to be investigated.

Accurate loss models are crucial in order to increase the power density and/or the efficiency of inductive components. There are publications focussing on model inductive components [1]–[6]. The aim of this paper is to improve the model accuracy. This is achieved by combining the best state-of-the-art approaches and by embedding newly-developed approaches into a novel loss calculation framework. All the equations required and each step are explained in such a way that a tutorial presentation of this topic arises.

Core loss modeling will be shown in **Section II**, winding loss models in **Section III**, and experimental results in **Section IV**.

II. CORE LOSS MODELING

There are basically three physical loss sources: (static) hysteresis losses, eddy-current losses, and a third loss component which is often referred to as residual losses. Hysteresis losses are linear with the frequency f (rate-independent B-H loop). Eddy-current losses occur because of an induced current due to the changing magnetic field and are strongly dependent on the material conductivity and the core geometry. The residual losses are, according to [7], due to relaxation processes: if the thermal equilibrium of a magnetic system changes, the system progressively moves towards the new thermal equilibrium condition. When the magnetization changes rapidly, as for example is the case in high-frequency or pulsed field applications, such relaxation processes become very important.

Core losses have to be described as a function of the peak-to-peak flux density ΔB, frequency f, DC premagnetization H_{DC}, temperature T, core shape, flux waveform, and material. This is not a straight forward process; predicting core losses is a difficult challenge.

A. State-of-the-art approaches for core loss calculation

The most used equation for characterizing core losses is the empirical power equation [8]

$$P_v = k f^\alpha \hat{B}^\beta \qquad (1)$$

where $\hat{B}$ is the peak induction of a sinusoidal excitation with frequency f, P_v is the time-average power loss per unit volume, and k, α, β are material parameters that have to be empirically determined. The equation is called the Steinmetz Equation SE (after Charles P. Steinmetz). The material parameters k, α, and β are accordingly referred to as the Steinmetz parameters. They are valid for a limited frequency and flux density range. Core manufacturers often provide data of losses per volume (or per weight) as a function of frequency f, flux density $\hat{B}$, and temperature T. Out of this data the Steinmetz parameters can be extracted. Sometimes, the Steinmetz parameters are quoted. However, the SE is, in many circumstances, not capable of accurately calculating core losses because

- the material is usually exposed to non-sinusoidal flux waveforms in power electronic applications,
- and a potential DC premagnetization H_{DC} is not considered.

Different approaches have been developed to overcome this limitation and determine losses for a wider variety of waveforms. The analysis in [9], for instance, is motivated by the fact that the loss due to domain wall motion has a direct dependency of dB/dt. As a result, a modified Steinmetz Equation is proposed. In [10] the approach is further improved

and in [11] a method of dealing with minor hysteresis loops is introduced and some minor changes to the equation are made. The approach of [9], [10], and [11] leads to the improved Generalized Steinmetz Equation (iGSE)

$$P_{\mathrm{v}} = \frac{1}{T} \int_0^T k_i \left| \frac{\mathrm{d}B}{\mathrm{d}t} \right|^\alpha (\Delta B)^{\beta - \alpha} \, \mathrm{d}t \qquad (2)$$

where ΔB is peak-to-peak flux density and

$$k_i = \frac{k}{(2\pi)^{\alpha - 1} \int_0^{2\pi} |\cos \theta|^\alpha 2^{\beta - \alpha} \mathrm{d}\theta}. \qquad (3)$$

The parameters k, α, and β are the same parameters as used in the SE (1). The losses of any flux waveform can be calculated without requiring extra characterization of material parameters beyond those for the SE when using the iGSE. This approach is widely applied [2], [12]. In [2] it has been evaluated as the most accurate state-of-the-art loss model based on Steinmetz parameters. However, during the phase of constant flux (where the voltage across the magnetic component is zero) losses still may occur in the core material. This is in contradiction to (2). Losses still occur a short period after switching the winding voltage to zero due to magnetic relaxation. In [13] a further improvement of the iGSE that takes this effect into consideration is suggested and accordingly named i²GSE

$$P_{\mathrm{v}} = \frac{1}{T} \int_0^T k_i \left| \frac{\mathrm{d}B}{\mathrm{d}t} \right|^\alpha (\Delta B)^{\beta - \alpha} \, \mathrm{d}t + \sum_{l=1}^n Q_{\mathrm{r}l} P_{\mathrm{r}l}, \qquad (4)$$

where $P_{\mathrm{r}l}$ is calculated for each stepped voltage change according to

$$P_{\mathrm{r}l} = \frac{1}{T} k_{\mathrm{r}} \left| \frac{\mathrm{d}}{\mathrm{d}t} B(t) \right|^{\alpha_{\mathrm{r}}} (\Delta B)^{\beta_{\mathrm{r}}} \left(1 - \mathrm{e}^{-\frac{t_1}{\tau}} \right), \qquad (5)$$

and $Q_{\mathrm{r}l}$ is a function that further describes the voltage change and is

$$Q_{\mathrm{r}l} = \mathrm{e}^{-q_{\mathrm{r}} \left| \frac{\mathrm{d}B(t_+)/\mathrm{d}t}{\mathrm{d}B(t_-)/\mathrm{d}t} \right|}, \qquad (6)$$

and α, β, k_i, α_{r}, β_{r}, k_{r}, τ, and q_{r} are material parameters. The parameters are valid only for a limited frequency and flux density range.

The approach of (4) attempts to solve the problem of different flux shapes. However, (4) does not consider a potential DC premagnetization H_{DC}. For many materials, the impact of a DC bias cannot be neglected as it may increase the losses by a factor of more than two [14]. A means of considering DC bias losses is suggested in [15]: the effect of a DC bias is modeled by the given ratio between losses with and without DC bias for different DC bias levels H_{DC} and different AC flux densities. This ratio is called the displacement factor DPF. A graph that shows the DPF for the material ferrite N87 from EPCOS is shown in [15]. In [9] an empirical formula that describes the DPF is given (although it is not labeled as DPF). According to [9], [15] the DPF does not depend on the frequency f and can be described as a function of the AC flux density and the DC bias H_{DC}. A similar approach is suggested in [16]. The approaches of [9], [15], [16] have in common that a factor is introduced by which the calculated losses have to be multiplied to take a premagnetization into consideration. In other words,

the parameter k_i of (4) is multiplied by the DPF and therewith becomes dependent on ΔB. Another means of describing core losses under DC bias condition is shown in [14]: a graph that shows the dependency of the Steinmetz parameters (α, β and k_i) on premagnetization is introduced. The graph is named the Steinmetz Premagnetization Graph SPG. This enables the calculation of losses via the Steinmetz equation (1), the iGSE (2), or the i²GSE (4) using appropriate Steinmetz parameters.

A core loss calculation with the models, such as i²GSE, SPG, or DPF, described above has one major drawback: the models are based on parameters that cannot be extracted from the data provided by the core manufacturers. Until core manufacturers provide data to extract the dependency of a DC bias, e.g. an SPG, or provide data with which to predict relaxation effects, e.g. relaxation parameters α_{r}, β_{r}, k_{r}, τ, and q_{r} of (5) and (6), core loss measurements must be performed for an accurate core loss calculation. The measurement results could be stored in a core material database that enables all the effects described above to be considered when designing inductive components. This has been one aim of this work: to determine a structure for a core material database (later named loss map) to permit accurate core loss calculations. A core loss measurement test setup has been built for this purpose and is described in Appendix A.

B. Loss map

As mentioned above, until core manufacturers provide data for loss calculation based on i²GSE, SPG, or DPF, core losses can be calculated with a loss map that is based on measurements. This loss map stores the loss information for different operating points, each described by the flux density ripple ΔB, the frequency f, the temperature T, and a DC bias H_{DC}. This has been implemented e.g. in [17]–[19]. This approach is independent of a parameter set, e.g. Steinmetz parameter set, hence a higher accuracy over a wide frequency and flux density range can be expected as the problem that Steinmetz parameters are only valid for a limited frequency and flux density range does not occur. A novel loss map structure has been developed for this work and will be presented within this Subsection.

The loss map stores loss densities (in our case, loss per volume) as the data should be applicable for all different kinds of core shapes. A core with homogenous flux density distribution is basically needed for measuring loss densities. This would be the case when having an "ideal" toroid with very small radial thickness. If the radial thickness is not small, the flux density is not distributed homogenously over the radius and the core property is more complicated. In this case "effective" dimensions (effective length l_{e} and effective cross-sectional area A_{e}) are needed that permits calculation as if it were an ideal toroid. The core losses per volume can then be extracted by dividing the measured losses by the effective volume of the core $V_{\mathrm{e}} = A_{\mathrm{e}} l_{\mathrm{e}}$. These effective dimensions for a toroid are [8]

$$A_{\mathrm{e}} = \frac{h \ln^2 r_2/r_1}{1/r_1 - 1/r_2}, \qquad (7)$$

Fig. 1. Content of loss map.

Fig. 2. Illustration of breaking a flux waveform into its components.
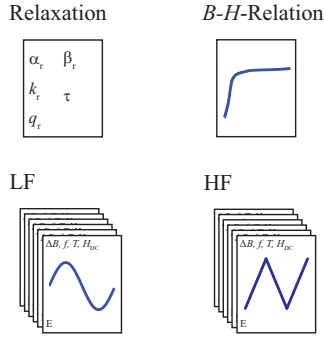
and

$$l_e = \frac{2\pi \ln r_2/r_1}{1/r_1 - 1/r_2},\qquad(8)$$

where h is the height, r_1 is the inner radius, and r_2 is the outer radius of the toroid. These values are usually given by the core manufacturer. In the case of general core shapes, [8] proposes a method of how to find these dimensions l_e and A_e, such that one can perform inductance calculations as if it were an ideal toroid. In this general case the effective dimensions are only useful for calculating the inductance value and not for core loss calculation. This is because the flux density may not be the same at every position of the core. Calculating the losses for a toroid with the equivalent dimensions is possible due to the uniformity of the flux density.

After it has been clarified on what cores measurements for setting up a loss map can be performed, it has to be further discussed what type of waveforms are to be measured. In some applications, e.g. Power Factor Correction (PFC), a high frequency (piecewise-linear) flux ripple is superimposed to a low frequency (sinusoidal) flux waveform. This well illustrates the typical situation in modern power electronic systems: the low frequency fundamental waveform usually has a sinusoidal shape, while the high frequency ripple consists of piecewise-linear phases. The B-H-loop of the low frequency fundamental flux part is called the major loop, while the high frequency loops are called minor loops. According to [6], [11] the loops can be separated into major and minor loops and then the losses can be independently calculated for each loop. This has been verified by experiments. Loss information for different operating points are stored in the loss map, each described by the flux density ripple ΔB, the frequency f, the temperature T, and a DC bias H_{DC}. On the basis of the above discussion, sinusoidal waveform measurement results are stored for frequencies below $1\,\mathrm{kHz}$ and triangular, i.e. piecewise-linear, waveform measurement results are stored for frequencies above $1\,\mathrm{kHz}$. In addition, the loss database stores the initial B-H curve, which can, for example, be taken from the data sheet, and one set of relaxation parameters α_r, β_r, k_r, τ, and q_r is stored. The extraction of the relaxation parameters has been carried out as described in [13]. The initial B-H curve enables to introduce a reluctance model that takes the non-linearity of the core material into consideration (cf. Subsecti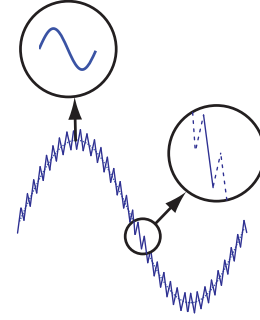on II-D). The relaxation parameters permit to take relaxation effects into consideration by using the i²GSE (4). In Fig. 1 an overview of the loss map content is illustrated.

C. Use of loss map

The applied core loss approach in this work can be described as a hybrid of the Steinmetz approach and a loss map approach: a loss map is taken according to the discussion in the previous section; the interpolation and extrapolation between operating points is then made with the SE or the i²GSE. This novel approach of core loss modeling will be described within this Subsection.

The flux density waveform for which the losses have to be calculated could, for instance, be simulated in a circuit simulator. This simulated waveform is then broken up into its fundamental (mostly sinusoidal) flux waveform and into piecewise linear flux waveform segments, as illustrated in Fig. 2. The loss energy is then derived for all segments, summed-up and divided by the fundamental period length. The piecewise-linear waveforms are translated into a symmetric triangular flux waveform with the same peak-to-peak flux density ΔB, the same flux density slope $\mathrm{d}B/\mathrm{d}t$ and the same DC premagnetization H_{DC}, resulting in a symmetric triangular operating point that is defined as $(\Delta B^*,\ f^*,\ H_{DC}^*,\ T^*)$. The translation is necessary as the loss map stores operating points of symmetric triangular waveforms. How the loss map extraction is implemented will be explained next.

The losses to the (sinusoidal or triangular flux waveform) operating point $(\Delta B^*,\ f^*,\ H_{DC}^*,\ T^*)$ are calculated by the following steps:

1) The close-by operating points of the loss map have to be found. Nine operating points are necessary for the interpolation: three for the interpolation of f and ΔB, multiplied by three for the interpolation of the temperature T and DC magnetic field strength H_{DC}. This is illustrated in Fig. 3 and will be discussed below.

2) In a second step, a linear interpolation for the temperature T and the DC magnetic field strength H_{DC} is performed. This is illustrated in Fig. 3(a) and carried out for each pair $\Delta B/f$. Therefore the following points are derived: $(\Delta B_1, f_1, H_{DC}^*, T^*)$, $(\Delta B_2, f_1, H_{DC}^*, T^*)$, $(\Delta B_1, f_2, H_{DC}^*, T^*)$, i.e. three operating points remain with inter-/extrapolated temperature T and magnetic field strength H_{DC}.
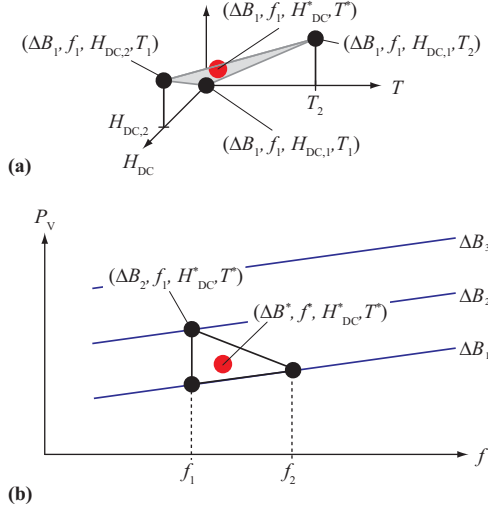
Fig. 3. Illustration of interpolation.

3) The peak-to-peak flux density ΔB and the frequency f are inter/extrapolated by extracting the Steinmetz Parameters from the three remaining operating points and calculating the losses by the SE (in the case of a sinusoidal flux waveform) or the i^{2}GSE (in the case of a piecewise linear waveform). This is illustrated in Fig. 3(b). The relaxation term of the i^{2}GSE can directly be evaluated with the relaxation parameters from the loss map; for it, information about the antecedent piecewise-linear flux phase is required.

This hybrid approach already enables a high degree of accuracy for a limited number of pre-measured operating points in the loss map as the inter/extrapolation by the SE or i^{2}GSE takes the basic core loss behavior into account.

D. Effect of core shape

The final aspect to be considered in core loss calculation is the effect of the core shape/size. Simply multiplying the loss density with the effective dimensions A_e and l_e of the core leads in many cases to incorrect loss values. This is, as stated before, due to the flux density being not necessarily uniform at every position in the core. By introducing a reluctance model of the core, and with it, calculating the flux density in every core section of (approximately) homogenous flux density, one can calculate the losses of each section. The core losses of each section are then summed-up to obtain the total core losses. How to set up a reluctance model, including an accurate air gap reluctance, is shown in [20]. Saturation effects can be taken into consideration by varying the relative permeability μ_r according to the B-H curve from the loss map.

III. Winding Loss Modeling

The second source of losses in inductive components are the ohmic losses in the windings. The resistor of a conductor increases with increasing frequency due to eddy currents. Self-induced eddy currents inside an inductor lead to the skin effect. Eddy currents due to an external alternating magnetic field,
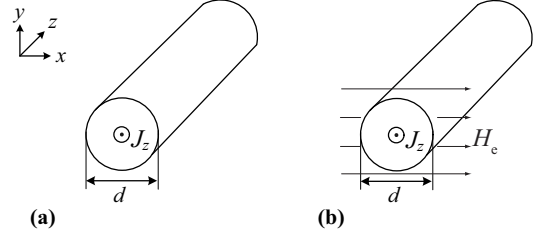

Fig. 4. Cross-section of the round conductor considered with a current in z-direction. The conductor is infinitely large in z-direction.

e.g. the air gap fringing field or the magnetic field from other conductors, lead to the proximity effect.

The skin effect losses (including DC losses) per unit length in round conductors (cf. Fig. 4(a)) can be calculated as [21]

$$P_S = R_{DC} \cdot F_R(f) \cdot \hat{I}^2 \qquad (9)$$

with $\delta = \frac{1}{\sqrt{\pi \mu_0 \sigma f}}$, $\xi = \frac{d}{\sqrt{2}\delta}$, $R_{DC} = \frac{4}{\sigma \pi d^2}$, and[1]

$$F_R = \frac{\xi}{4\sqrt{2}} \left(\frac{\mathrm{ber}_0(\xi)\mathrm{bei}_1(\xi) - \mathrm{ber}_0(\xi)\mathrm{ber}_1(\xi)}{\mathrm{ber}_1(\xi)^2 + \mathrm{bei}_1(\xi)^2} \right.$$
$$\left. - \frac{\mathrm{bei}_0(\xi)\mathrm{ber}_1(\xi) + \mathrm{bei}_0(\xi)\mathrm{bei}_1(\xi)}{\mathrm{ber}_1(\xi)^2 + \mathrm{bei}_1(\xi)^2} \right). \qquad (10)$$

δ is commonly named the skin depth, f is the frequency, d is the conductor diameter, and σ is the electric conductivity of the conductor material. The proximity effect losses in round conductors (cf. Fig. 4(b)) per unit length can be calculated as [21]

$$P_P = R_{DC} \cdot G_R(f) \cdot \hat{H}_e^2 \qquad (11)$$

with

$$\delta = \frac{1}{\sqrt{\pi \mu_0 \sigma f}}, \qquad (12)$$

$\xi = \frac{d}{\sqrt{2}\delta}$, $R_{DC} = \frac{4}{\sigma \pi d^2}$, and

$$G_R = - \frac{\xi \pi^2 d^2}{2\sqrt{2}} \left(\frac{\mathrm{ber}_2(\xi)\mathrm{ber}_1(\xi) + \mathrm{ber}_2(\xi)\mathrm{bei}_1(\xi)}{\mathrm{ber}_0(\xi)^2 + \mathrm{bei}_0(\xi)^2} \right.$$
$$\left. + \frac{\mathrm{bei}_2(\xi)\mathrm{bei}_1(\xi) - \mathrm{bei}_2(\xi)\mathrm{ber}_1(\xi)}{\mathrm{ber}_0(\xi)^2 + \mathrm{bei}_0(\xi)^2} \right). \qquad (13)$$

Here, R_{DC} is the resistor per unit length, hence the losses P_S and P_P are losses per unit length as well.

The external magnetic field strength H_e of every conductor has to be known when calculating the proximity losses. In the case of an un-gapped core and windings that are fully-enclosed by core material, 1D approximations to derive the magnetic field exist. The most popular method is the Dowell method [23]. However, in the case of gapped cores, such 1D approximations are not applicable as the fringing field of the air gap cannot be described in an 1D manner. An approach

---

[1]The solution is based on a *Bessel differential equation* that has the form $x^2 y'' + x y' + (k^2 x^2 - v^2) y = 0$. With the general solution $y = C_1 \mathbb{J}_v(kx) + C_2 \mathbb{Y}_v(kx)$, whereas $\mathbb{J}_v(kx)$ is known as *Bessel function of the first kind and order* v and $\mathbb{Y}_v(kx)$ is known as *Bessel function of the second kind and order* v [22]. Furthermore, to resolve $\mathbb{J}_v(kx)$ into its real- and imaginary part, the *Kelvin functions* can be used: $\mathbb{J}_v(\mathrm{j}^{\frac{3}{2}}x) = \mathrm{ber}_v x + \mathrm{j}\,\mathrm{bei}_v x$.
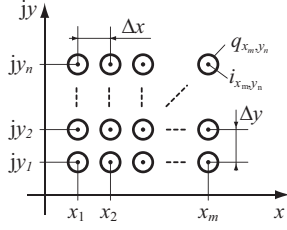
(a)
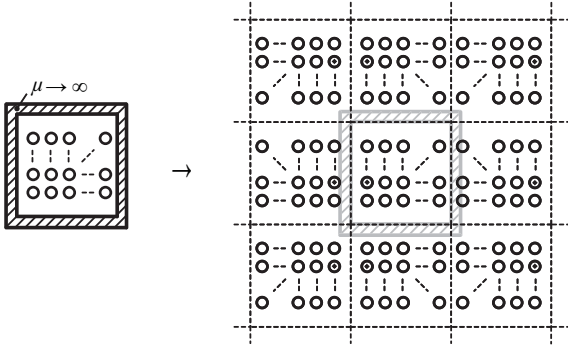
(b)

Fig. 5. **(a)** Illustration of winding arrangement. **(b)** Illustration of mirroring.

has to be selected/derived to overcome these limitations. The following approach can be used for inductive components with and without air gaps.

A winding arrangement as illustrated in Fig. 5(a) leads to an external field vector $\hat{\mathbf{H}}_e$ across conductor q_{x_i,y_k} due to the current $\hat{i}_{x_u,y_l}$ of conductor q_{x_u,y_l} of

$$
\begin{aligned}
\hat{\mathbf{H}}_e = & -\mathrm{j}\frac{\hat{i}_{x_u,y_l}}{2\pi\sqrt{(x_u-x_i)^2+(y_l-y_k)^2}} \\
& \cdot \frac{(x_u-x_i)+\mathrm{j}(y_l-y_k)}{\sqrt{(x_u-x_i)^2+(y_l-y_k)^2}} \\
= & \frac{\hat{i}_{x_u,y_l}\left((y_l-y_k)-\mathrm{j}(x_u-x_i)\right)}{2\pi\left((x_u-x_i)^2+(y_l-y_k)^2\right)}.
\end{aligned}
\tag{14}
$$

Complex numbers are used to identify the conductor position as this simplifies the calculation. The magnitude of the total external field $\hat{H}_e$ across conductor q_{x_i,y_k} can be calculated with

$$
\hat{H}_e = \left| \sum_{u=1}^{m}\sum_{l=1}^{n} \epsilon(u,l)\frac{\hat{i}_{x_u,y_l}\left((y_l-y_k)-\mathrm{j}(x_u-x_i)\right)}{2\pi\left((x_u-x_i)^2+(y_l-y_k)^2\right)} \right|,
\tag{15}
$$

where $\epsilon(u,l) = 0$ for $u = i$, $l = k$ and $\epsilon(u,l) = 1$ for $u \neq i$, $l \neq k$. With the derived external magnetic field $\hat{H}_e$ the proximity effect losses can be calculated based on (11).

The impact of a magnetic conducting material can be modeled with the *method of images*. The wall can be replaced by injected currents as the magnetic H-field is always perpendicular to a magnetic wall with infinite permeability [1]. The new currents are the mirrored version of the original currents,
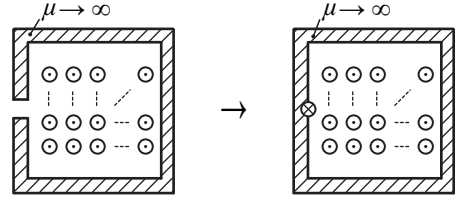

Fig. 6. Illustration of modeling an air gap as a fictitious conductor.

as illustrated in Fig. 5(b). In case of windings that are fully-enclosed, the opposite wall is mirrored as well, thus a new wall is created. The mirroring can be continued to pushing the walls away. This is illustrated in Fig. 5(b). For this work, the mirroring has been stopped after the material was replaced by conductors three times in each direction.

The presence of an air gap can be modeled as a fictitious conductor without eddy currents equal to the magneto-motive force (mmf) across the air gap [1]. This situation is illustrated in Fig. 6. The polarity of the fictitious current is opposed to the conductor polarity. Please note that as soon as the material is replaced by injected currents, the fictitious air gap current doubles as it is mirrored.

In the case of an E-core, for instance, the winding losses have to be calculated differently for each section illustrated in Fig. 7 as the mirroring leads to different results.
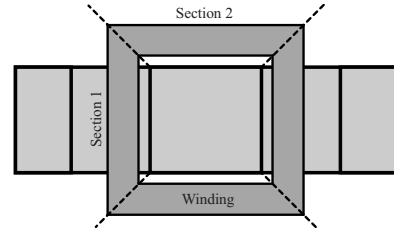

Fig. 7. Illustration of different sections in the winding path of an E-core.

In the case of a non-sinusoidal current it is permissible to express the current as a Fourier series, calculate the losses for each frequency independently, and then total them up. It is also permissible to total up the independently calculated skin-effect and proximity-effect losses [24].

It is possible to accurately model winding losses of solid conductors based on the above discussion. In Subsection III-B a discussion about the expected accuracy and comparisons with FEM simulations is presented. Based on the above derivations, a litz wire calculation is also possible, which will be shown in the following Subsection III-A.

A. Litz-wire windings

Winding losses can be reduced by using litz-wire windings. Litz-wire windings are made up of multiple individually-insulated strands as illustrated in Fig. 8. In litz-wire windings, skin and proximity effects can be further divided into strand-level and bundle-level effects [25]. The effect related to eddy currents circulating in paths involving multiple strands is called the bundle-level effect, whereas strand-level effects take
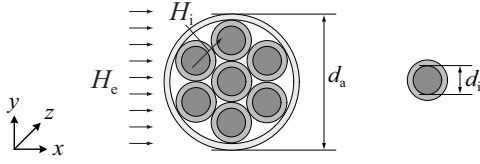
Fig. 8. Cross-sectional area of litz-wire winding.

place within individual strands. The strands are twisted such that each strand equally occupies each position in the bundle. Therewith, bundle-level effects can be strongly reduced and are neglected in the following derivations.

The skin-effect losses, including DC losses, of a litz-wire winding that consists of n strands, each with strand diameter d_i are calculated as [26], [27]

$$P_{S,L} = n \cdot R_{DC} \cdot F_R(f) \cdot \left(\frac{\hat{I}}{n} \right)^2, \qquad (16)$$

where $R_{DC} = \frac{4}{\sigma \pi d_i^2}$, and $F_R(f)$ is calculated as (10) with the strand diameter $d = d_i$.

The magnetic field that leads to proximity losses is the sum of the external magnetic field H_e and the internal magnetic field H_i. The external magnetic field H_e originates in the air gap fringing field or the magnetic field from the neighboring conductors and can be calculated in the same manner as described for the case of solid conductors. The internal magnetic field H_i across one strand originates in its neighboring strands. It is assumed that the current is equally distributed over the litz-wire cross-sectional area for the calculation of the internal magnetic field.

The proximity losses in litz-wire windings can then be calculated as [26], [27]

$$\begin{aligned} P_{P,L} &= P_{P,L,e} + P_{P,L,i} \\ &= n \cdot R_{DC} \cdot G_R(f) \left(\hat{H}_e^2 + \frac{\hat{I}^2}{2\pi^2 d_a^2} \right) \end{aligned} \qquad (17)$$

where $R_{DC} = \frac{4}{\sigma \pi d_i^2}$, and $G_R(f)$ is calculated as (13) with the strand diameter $d = d_i$.

B. Accuracy analysis

The formulas derived in the last Subsections are based on analytical equations. The major simplification that has been made is to neglect the magnetic field of the induced eddy currents. The derived field H_e is assumed to penetrate completely thorough the conductors. According to [1] this approximation is valid if the largest dimension of the conductor, i.e. the diameter for a round conductor/strand, is less than 1.6 times the skin depth δ. Consequently, with (12) the frequency f_{max}, up to which the calculation for a given conductor diameter d is accurate, can be calculated as

$$f_{max} = \frac{2.56}{\pi \mu_0 \sigma d^2}. \qquad (18)$$

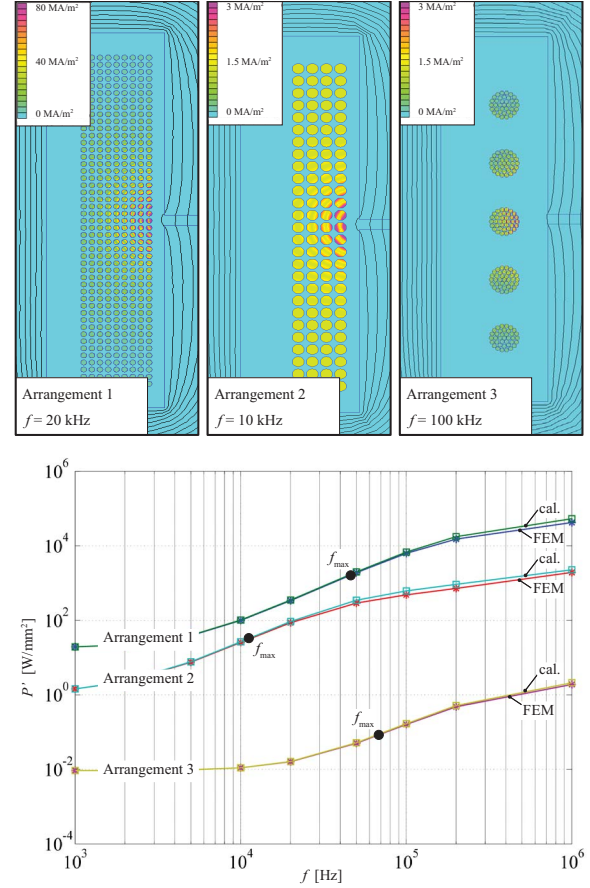Three winding arrangements have been calculated and compared to 2D FEM simulations. The FEM simulations have

Fig. 9. Comparison of winding calculation to FEM simulation. Size of core window: 37 mm x 10.15 mm. Air gap length 1 mm. Winding arrangement 1: number of turns $N = 423$; $\hat{I} = 1$ A; winding diameter $d = 0.5$ mm. Winding arrangement 2: number of turns $N = 108$; $\hat{I} = 1$ A; winding diameter $d = 1$ mm. Winding arrangement 3: number of turns $N = 5$; number of strands $n = 37$; $\hat{I} = 1$ A; strand diameter $d_i = 0.4$ mm.

been carried out with the software FEMM[2]. The results are given in Fig. 9. Simulations for frequencies below f_{max} lead to deviations of always less than 5 %, above f_{max} more than 5 %, but, in all illustrated cases, never more than 25 %.

IV. EXPERIMENTAL RESULTS

Loss measurements on an inductor have been conducted to verify the loss calculations. The inductor has been built with two E-cores having an air gap in the center leg (EPCOS Ferrite N27; Core E55/28/21; air gap length $l_g = 1$ mm [28]). The windings are made of a wire of solid copper with diameter 1.7 mm. The number of turns has been $N = 18$. A photo of the inductor is given in Fig. 10. The measurements have been carried out with a Yokogawa WT3000 Precision Power Analyzer.

Two different types of loss measurements have been performed and compared to loss calculations. The first type of measurements have been conducted with symmetric triangular flux waveforms at different operating points to which the results are given in Table I. The second type of measurements

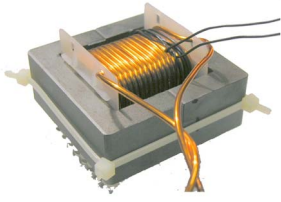[2]FEMM 4.2, freeware from www.femm.info.

Fig. 10. E-core type 1 used for both measurements

have been conducted with a low frequency LF (100 Hz) sinusoidal current with a superimposed high frequency HF (10 kHz) triangular switching ripple. A low modulation index has been chosen, hence the high frequency peak-to-peak flux density ΔB_{HF} is (almost) constant over the full low frequency period. The results of the second measurement are given in Table II. A high level of accuracy with a deviation of max. 10 % has been achieved.

V. CONCLUSION AND FUTURE WORK

This publication investigated loss models of inductive components. The impact of peak-to-peak flux density ΔB, frequency f, DC premagnetization, temperature, core shape, minor and major loops, flux waveform, and material on core loss calculation have been considered. Formulas for round conductors and litz wires, each including skin- and proximity effects (including the effect of an air gap fringing field) are given for calculating winding losses. A high level of accuracy has been achieved by combining the best state-of-the-art approaches and by embedding newly-developed approaches into a novel loss calculation framework. The high level of accuracy has been proven with measurements on an E-core inductor.

When designing magnetic components another important aspect is the expected temperature of the component. This is not only important to avoid thermal problems, it has also importance for a correct loss modeling since the core and winding losses are influenced by the temperature. Hence, a thermal model is indispensable for an accurate loss model. A thermal model should be derived in addition to the work presented in this paper.

APPENDIX A
TEST-SETUP FOR MEASURING CORE LOSSES

In order to perform core loss measurements the best measurement technique has to be selected first. In [29] different methods are compared. The B-H Loop Measurement has been evaluated as the most suitable. Amongst other advantages, this technique offers rapid measurement (compared to other methods, e.g. calorimetric measurements), copper losses are not measured, and a good accuracy. The principle is as follows: two windings are placed around the Core Under Test (CUT). The sense winding (secondary winding) voltage v is integrated to sense the core flux density B

$$B(t) = \frac{1}{N_2 \cdot A_{\mathrm{e}}} \int_0^t v(\tau) \mathrm{d}\tau \qquad (19)$$

(a)
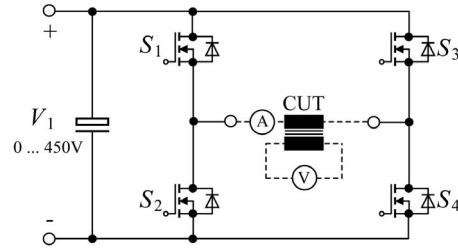
(b)

Fig. 11. Test setup (a) photograph, (b) simplified schematic.

where N_2 is the number of sense winding turns and A_{e} is the effective core cross-section of the CUT. The current in the excitation winding (primary winding) is proportional to the magnetic field strengths H

$$H(t) = \frac{N_1 \cdot i(t)}{l_{\mathrm{e}}} \qquad (20)$$

where N_1 is the number of excitation winding turns and l_{e} is the effective magnetic path length of the CUT. The loss per unit volume is then the enclosed area of the B-H loop multiplied by the frequency f

$$\frac{P}{V} = f \oint H \mathrm{d}B. \qquad (21)$$

The selected approach is widely used [11], [18], [30], [31]. The built test system consists of a power stage, a power supply, an oscilloscope and a heating chamber. It is controlled by a MATLAB program running on the oscilloscope under Microsoft Windows. In Fig. 11 a photograph (a) and the simplified schematic (b) of the power stage are shown. The power stage is capable of a maximal input voltage of 450 V, output current of 25 A and a switching frequency of up to 200 kHz. The test set-up allows application of a general rectangular voltage shape across the CUT that leads to a triangular and/or trapezoidal current shape including a DC bias (if desired). The current is sensed by a DC current transducer to control the DC current. A low frequency sinusoidal excitation is also possible; an output filter has been designed to achieve a sinusoidal current/voltage shape for frequencies up to 1 kHz.

The reader is referred to [14] for more information about the test-setup, including a detailed accuracy analysis of the loss measurement.

<div align="center">

TABLE I

RESULTS OF MEASUREMENT 1

</div>

Operating Points				Calculated Losses			Measured Losses	Comparison
ΔB [T]	f [kHz]	Duty-Cycle	H_{DC} [A/m]	Core Losses [W]	Winding Losses [W]	Total Losses [W]	Total Losses [W]	Rel. Error [%]
0.25	1	0.5	0	0.06	0.11	0.17	0.18	-5.56
0.5	1	0.5	0	0.32	0.42	0.74	0.77	-3.90
0.25	2	0.5	0	0.14	0.12	0.26	0.27	-3.70
0.5	2	0.5	0	0.72	0.49	1.21	1.21	0.00
0.25	5	0.5	0	0.4	0.23	0.63	0.61	3.28
0.5	5	0.5	0	2.04	0.92	2.96	2.70	9.63

<div align="center">

TABLE II

RESULTS OF MEASUREMENT 2

</div>

Operating Points			Calculated Losses			Measured Losses	Comparison
$\hat{I}_{LF}$ [A]	ΔB_{LF} [T]	ΔB_{HF} [T]	Core Losses [W]	Winding Losses [W]	Total Losses [W]	Total Losses [W]	Rel. Error [%]
5	0.25	0.15	0.44	0.35	0.79	0.76	3.95
10	0.5	0.3	1.83	1.51	3.35	3.6	-6.94

REFERENCES

[1] A. V. den Bossche and V. C. Valchev, *Inductors and Transformers for Power Electronics*. CRC Press, Taylor & Francis Group, 2005.

[2] I. Villar, U. Viscarret, I. Etxeberria-Otadui, and A. Rufer, "Global loss evaluation methods for nonsinusoidally fed medium-frequency power transformers," *IEEE Transactions on Industrial Electronics*, vol. 56, pp. 4132–4140, Oct. 2009.

[3] R. Petkov, "Optimum design of a high-power, high-frequency transformer," *IEEE Transactions on Power Electronics*, vol. 11, pp. 33 –42, Jan. 1996.

[4] T. Komma, *Allgemein gültiger Entwurfsalgorithmus für magnetische Komponenten in Schaltnetzteilen mit unterschiedlichen Topologien und Schaltfrequenzen bis 2 MHz*. PhD thesis, Technische Universität Dresden, 2005.

[5] P. Wallmeier, *Automatisierte Optimierung von induktiven Bauelementen für Stromrichteranwendungen*. PhD thesis, Universität - Gesamthochschule Paderborn, 2001.

[6] A. Brockmeyer, *Dimensionierungswerkzeug für magnetische Bauelemente in Stromrichteranwendungen*. PhD thesis, RWTH Aachen, 1997.

[7] J. B. Goodenough, "Summary of losses in magnetic materials," *IEEE Transaction on Magnetics*, vol. 38, pp. 3398–3408, Sept. 2002.

[8] E. C. Snelling, *Soft Ferrites, Properties and Applications*. 2nd edition, Butterworths, 1988.

[9] J. Reinert, A. Brockmeyer, and R. De Doncker, "Calculation of losses in ferro- and ferrimagnetic materials based on the modified Steinmetz equation," *IEEE Transactions on Industry Applications*, vol. 37, no. 4, pp. 1055–1061, 2001.

[10] J. Li, T. Abdallah, and C. R. Sullivan, "Improved calculation of core loss with nonsinusoidal waveforms," in *Industry Applications Conference, 2001. 36th IEEE IAS Annual Meeting.*, vol. 4, pp. 2203–2210, 2001.

[11] K. Venkatachalam, C. R. Sullivan, T. Abdallah, and H. Tacca, "Accurate prediction of ferrite core loss with nonsinusoidal waveforms using only Steinmetz parameters," in *Proc. of IEEE Workshop on Computers in Power Electronics*, pp. 36–41, 2002.

[12] J. Biela, U. Badstuebner, and J. W. Kolar, "Impact of power density maximization on efficiency of DC-DC converter systems," *IEEE Transactions on Power Electronics*, vol. 24, pp. 288–300, Jan. 2009.

[13] J. Mühlethaler, J. Biela, J. W. Kolar, and A. Ecklebe, "Improved core loss calculation for magnetic components employed in power electronic systems," in *Proc. of Applied Power Electronics Conference and Exposition (APEC)*, 2011.

[14] J. Mühlethaler, J. Biela, J. W. Kolar, and A. Ecklebe, "Core losses under DC bias condition based on Steinmetz parameters," in *Proc. of the IEEE/IEEJ International Power Electronics Conference (ECCE Asia)*, pp. 2430–2437, 2010.

[15] G. Niedermeier and M. Esguerra, "Measurement of power losses with DC-bias - The Displacement Factor," in *Proc. of PCIM*, pp. 169–174, 2000.

[16] A. Brockmeyer, "Experimental evaluation of the influence of DC-premagnetization on the properties of power electronic ferrites," in *Proc. of the 11th Annual Applied Power Electronics Conference (APEC).*, vol. 1, pp. 454–460, 3–7 March 1996.

[17] S. Iyasu, T. Shimizu, and K. Ishii, "A novel iron loss calculation method on power converters based on dynamic minor loop," in *Proc. of European Conference on Power Electronics and Applications*, pp. 2016–2022, 2005.

[18] T. Shimizu and K. Ishii, "An iron loss calculating method for AC filter inductors used on PWM inverters," in *Proc. of 37th IEEE Power Electronics Specialists Conference (PESC)*, pp. 1–7, 2006.

[19] K. Terashima, K. Wada, T. Shimizu, T. Nakazawa, K. Ishii, and Y. Hayashi, "Evaluation of the iron loss of an inductor based on dynamic minor characteristics," in *Proc. of European Conference on Power Electronics and Applications*, pp. 1–8, 2007.

[20] J. Mühlethaler, J. W. Kolar, and A. Ecklebe, "A novel approach for 3D air gap reluctance calculations," in *Proc. of the International Conference on Power Electronics - ECCE Asia*, 2011.

[21] J. Lammeraner and M. Stafl, *Eddy Currents*. Iliffe Books Ltd., 1966.

[22] L. C. Andrews, *Elementary Partial Differential Equations with Boundary Value Problems*. Academic Press College Division, 1986.

[23] P. Dowell, "Effects of eddy currents in transformer windings," *Proceedings of the Institution of Electrical Engineers*, vol. 113, no. 8, pp. 1387–1394, 1966.

[24] J. A. Ferreira, "Improved analytical modeling of conductive losses in magnetic components," vol. 9, pp. 127–131, Jan. 1994.

[25] C. Sullivan, "Optimal choice for number of strands in a litz-wire transformer winding," *IEEE Transactions on Power Electronics*, vol. 14, pp. 283 –291, Mar. 1999.

[26] J. A. Ferreira, *Electromagnetic Modelling of Power Electronic Converters*. Kluwer Academics Publishers, 1989.

[27] J. Biela, *Optimierung des elektromagnetisch integrierten Serien-Parallel-Resonanzkonverters mit eingeprägtem Ausgangsstrom*. PhD thesis, ETH Zurich, 2005.

[28] *Ferrites and Accessories, Edition 2007*. EPCOS AG.

[29] B. Carsten, "Why the magnetics designer should measure core loss; with a survey of loss measurement techniques and a low cost, high accuracy alternative," in *Proc. of PCIM*, pp. 163–179, 1995.

[30] F. Dong Tan, J. Vollin, and S. Cuk, "A practical approach for magnetic core-loss characterization," *IEEE Transactions on Power Electronics*, vol. 10, pp. 124–130, Mar. 1995.

[31] W. Shen, F. Wang, D. Boroyevich, and C. W. Tipton, "Loss characterization and calculation of nanocrystalline cores for high-frequency magnetics applications," *IEEE Transactions on Power Electronics*, vol. 23, pp. 475–484, Jan. 2008.